Frontiers of Information Technology & Electronic Engineering
www.jzus.zju.edu.cn; engineering.cae.cn; www.springerlink.com
ISSN 2095-9184 (print); ISSN 2095-9230 (online)
E-mail: jzus@zju.edu.cn

Review:

Millimeter-wave wireless communications for home network in fiber-to-the-room scenario

Chao HE‡[1], Zhixiong REN[1], Xiang WANG[1], Yan ZENG[1], Jian FANG[2], Debin HOU[3], Le KUAI[3], Rong LU[3], Shilin YANG[3], Zhe CHEN[3], Jixin CHEN[3]

[1]*Huawei Technologies Co. Ltd., Shenzhen 518129, China*

[2]*The State Radio Monitoring Center, Beijing 100037, China*

[3]*State Key Laboratory of Millimeter Waves, Southeast University, Nanjing 210096, China*

E-mail: charles.he@huawei.com; renzhixiong@huawei.com; eric.wangxiang@huawei.com; tony.zengyan@huawei.com; fangjian@srrc.org.cn; dbhou@seu.edu.cn; 230159362@seu.edu.cn; ronglu@seu.edu.cn; yang_shilinnudt@163.com; zhechen@seu.edu.cn; jxchen@seu.edu.cn

Received Aug. 30, 2020; Revision accepted Feb. 8, 2021; Crosschecked Mar. 3, 2021

Abstract: Millimeter-wave (mmWave) technology has been well studied for both outdoor long-distance transmission and indoor short-range communication. In the recently emerging fiber-to-the-room (FTTR) architecture in the home network of the fifth generation fixed networks (F5G), mmWave technology can be cascaded well to a new optical network terminal in the room to enable extremely high data rate communication (i.e., >10 Gb/s). In the FTTR+mmWave scenario, the rapid degradation of the mmWave signal in long-distance transmission and the significant loss against wall penetration are no longer the bottlenecks for real application. Moreover, the surrounding walls of every room provide excellent isolation to avoid interference and guarantee security. This paper provides insights and analysis for the new FTTR+mmWave architecture to improve the customer experience in future broadband services such as immersive audiovisual videos.

Key words: Fiber-to-the-room; Millimeter wave; Q-band; Cloud virtual reality (cloud VR); Home network; Beamforming; Radio frequency integrated circuit (RFIC)
https://doi.org/10.1631/FITEE.2000440 **CLC number:** TN923

1 Introduction

Over the past two decades, fixed broadband has been continuously developed to provide high-speed Internet connection for global end users.

In 1999, the Standardization Sector of the International Telecommunication Union (ITU-T) published the Asymmetric Digital Subscriber Line (ADSL) standard G.992.1 (ITU-T, 1999), opening the broadband era for this century. To evolve, the technologies over twisted pairs are further specified by the ITU-T, including VDSL2 G.993.2 (ITU-T, 2019c), G.fast (ITU-T, 2019a), and MGfast (ITU-T, 2020a) targeting to provide 10 Gb/s. However, fiber is considered to be a better medium for communication because of its much lower loss over long distances. The standards including gigabit-capable passive optical networks (GPON) G.984.1 (ITU-T, 2008), 10G-PON G.987.1 (ITU-T, 2016), and high-speed PON G.hsp (ITU-T, 2019b) that are aiming at 50 Gb/s connection over fiber have been specified. Because of the great advantage of low attenuation in fiber transmission, fiber access is becoming the dominant broadband access technology all over the world.

With the continuous expansion of the broadband access data rate (currently approaching multiple gigabits per second), high-resolution video services are becoming available and popular. Currently, over-the-

‡ Corresponding author
ORCID: Chao HE, https://orcid.org/0000-0001-6747-9245

top (OTT) media service platforms can supply customers with 4K and 8K videos, while multi-views even 360° augmented reality (AR) and virtual reality (VR) services are under investigation and tested through pilot usage. The quality of the home network (as in the "last ten meters connection") significantly influences the end user experience. User experiences are affected by many characteristics of the home network, e.g., maximum service throughput, stability and performance of the network, simple installation, and zero-touch management. To guarantee a good user experience, wireless local area network (WLAN) technologies, especially WiFi series, are some of the most widely deployed fixed wireless access technologies for the home network. The new published version of WLAN (802.11ax) is branded as WiFi 6, providing a maximum data rate around 10 Gb/s for end device connection. To form a backhaul network to support WiFi 6, ITU-T Q18/SG15 specified a new generation of wireline technology (G.hn2) (ITU-T, 2009) with 10-Gb/s data rate. In 2019, the European Telecommunications Standards Institute (ETSI) launched a new Industry Specification Group (ISG) F5G (ETSI, 2019) to explore the fifth generation of the fixed broadband, where 10G-PON and 802.11ax are the two main technology candidates for the access and home networks, respectively. Cloud VR is considered as a characteristic service.

Although a hybrid solution with G.hn2 and WiFi 6 may be a good option for satisfying the requirements of cloud VR, there are still many challenges. For example, because of the dynamic timeslot assignment and collision avoidance mechanism of a WiFi scheduler, the transmission latency cannot be well guaranteed against unexpected jitter of data rate and latency of the transmitted data flow. This makes it difficult to deploy time-sensitive or high data rate applications such as cloud VR, immersive real-time live broadcasting or gaming. It is expected in Zhang XZ et al. (2019) that for strong interactive ultimate cloud VR video transmission, a stable 4.4 Gb/s should be the minimum data rate while a stable 10 ms should be the maximum round-trip delay and jitter for the home network segment. A high-quality VR helmet is typically connected by a High-Definition Multimedia Interface (HDMI) cable which provides up to 40 Gb/s transmission capability. However, the connecting cable imposes critical physical restrictions to VR video/game customers for free movement, thus breaking the immersive live experience. To overcome this problem, fiber-to-the-room (FTTR) with millimeter-wave (mmWave) WLAN technology is then another candidate for better conveying service content in F5G (Fig. 1).

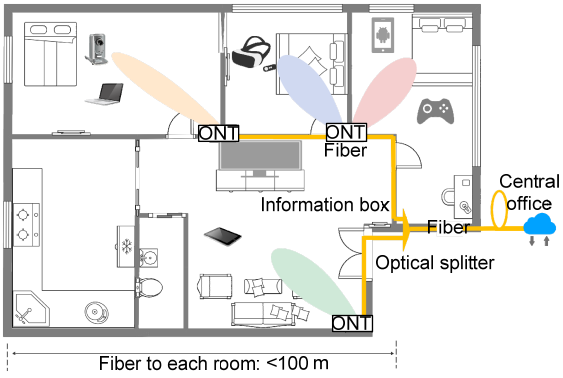

Fig. 1 Architecture schematic for fiber-to-the-room

In ITU-T, a new work item G.fin (ITU-T, 2020b) has been created to specify the system architecture, network functions, and transceiver specification over the fiber for home network. In addition, based on further fiber penetrating in the apartment for each room, using mmWave has two distinct advantages, i.e., more available spectrum leading to an extremely high speed and less interference between neighbor networks due to large insertion loss in penetrating walls (Marcus and Pattan, 2005). In the new architecture, each FTTR terminal can cascade with a mmWave access point (AP) in the downlink while connected to the same optical network terminal (ONT) in the uplink.

In the past two decades, there was a lot of good work on applying mmWave for home network to support immersive applications. For such a purpose, photonic devices and radio-over-fiber technology have been investigated (Hirata et al., 2006; Weiß et al., 2008; Guillory et al., 2011). Based on the home network scenarios and use cases, Genc et al. (2008) conducted investigations of the challenges of the 60-GHz mmWave transmission. Channel measurements and models at 45 and 60 GHz were studied (Sato et al., 1997; Moraitis and Constantinou, 2004; Wang H, 2015; Wu et al., 2017). In the 26-GHz band, Ai et al. (2017) carried out work on indoor massive multi-input multi-output (MIMO) measurement and

simulations. According to the nature of mmWave, the use of beamforming in short-range communication has been widely studied (Wang JY et al., 2009; Yu YK et al., 2011; Hur et al., 2013; Alkhateeb et al., 2014; Rangan et al., 2014); using this, capacity then can be further leveraged.

Short-range communication at 60 GHz has attracted much attention. Two early-stage developments are the releases of 802.11ad (IEEE, 2012) and 802.15.3c (IEEE, 2009). Owing to the high atmospheric absorption in this band (roughly −14 dB/km), it is not well suited for long-distance transmission. To overcome this problem, the China Wireless Personal Access Network (CWPAN) of the National Information Technology Standardization Committee (NITSC) developed Q-LINKPAN (the accompanying standard in IEEE is specified by the IEEE 802.11aj task group). This standard consists of two bands (i.e., 59–64 GHz and 43.5–47 GHz), the lower of which is based mainly on Q-LINKPAN-S. The Radio Management Bureau of China has published the regulation for systems operating in the band 42–48 GHz (Q-band) named "the usage of 40–50 GHz frequency band for mobile services in broadband wireless access systems" (MIIT, 2013). The main regulation parameters are shown in Table 1.

Table 1 Main regulation parameters for Q-band in China

Parameter	Value
Frequency band (GHz)	42.3–47, 47.2–48.4
Bandwidth (MHz)	540, 1080
Frequency tolerance	100×10^{-6}
Maximum transmit power at antenna port (dBm)	20
Maximum equivalent isotropic radiated power (EIRP) (dBm)	36

2 Q-band mmWave technologies

2.1 Baseband signal processing

IEEE 802.11aj defines two types of physical layer (PHY): one leverages the widely adopted orthogonal frequency division multiplexing (OFDM) while the other uses single-carrier (SC) modulation. OFDM PHY is well suited for frequency-selective wireless channels, but it has shortcomings such as high peak-to-average power ratio (PAPR), requiring dedicated power fallback in real applications. To avoid this problem, the SC mode is adopted as mandatory by IEEE 802.11aj technology. In addition, to overcome the multi-path shading effects caused by walls, human body, and furnishings, the MIMO scheme is preferred in 802.11aj rather than the beamforming in IEEE 802.11ad. Fig. 2 (IEEE, 2018) shows the processing blocks of the physical layer:

(1) Scrambler encodes the data blocks from the higher-level layer to reduce the probability of long zero sequences or one output bit sequences;

(2) Forward error coding (FEC) uses low-density parity-check code (LDPC) to enable error correction;

(3) Padding units fill the transmitted frames into an integral number of LDPC blocks;

(4) Stream sparser and inter-leaver divide the coded bits into blocks for each spatial stream;

(5) Constellation mapper maps the bit block in spatial streams to constellation points according to the selected modulation and coding scheme (MCS);

(6) Space-time block coding (STBC) encoder spreads the spatial distributed constellation points into spatial-temporal distributed streams;

(7) Cyclic shift block shifts different spatial streams to avoid unwanted beamforming effects;

(8) Guard interval inserting block implements padding fixed zero crossing sequences for symbols to against inter-symbol interference and track the channel changes;

(9) Pulse shaping filter shapes the signal spectrum to match the power spectrum density (PSD) requirements; Analog and radio frequency (RF) modules up-convert the baseband signal to the 45 GHz band channel and transmit signals within the regulated radio power.

The rate-dependent MCS parameters for 1080-MHz bandwidth with four spatial streams are shown in Table 2 (IEEE, 2018), where the roll-off

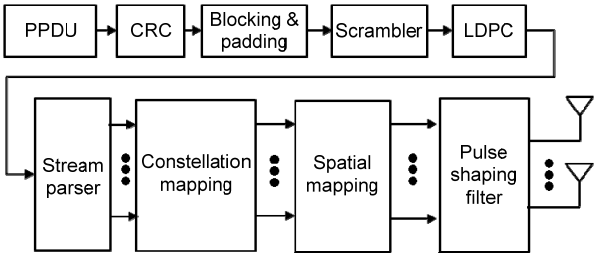

Fig. 2 Transmitter block diagram for data fields of CMMG SC mode PPDUs (IEEE, 2018)

Table 2 Data rates for different modulation and coding schemes (MCSs) and code rates (IEEE, 2018)

MCS	Modulation	Code rate	Data rate (Mb/s)
0	BPSK	1/2	1126.4
1	QPSK	1/2	2252.8
2	QPSK	3/4	3379.2
3	16-QAM	1/2	4505.6
4	16-QAM	3/4	6758.4
5	64-QAM	1/2	8448.0
6	64-QAM	3/4	10 137.6
7	64-QAM	13/16	10 982.4

factor of the pulse filter is 0.25. When the single-user 4×4 MIMO operation mode is selected, the maximum data rate is 14 Gb/s.

2.2 Radio frequency integrated circuit (RFIC) techniques and design

Millimeter-wave RFIC chipsets are essential components for supporting high-throughput transmission of Q-band signals. According to 802.11aj, to reach the highest data rate, the single channel bandwidth is set to be 1080 MHz with 64-QAM modulation. Furthermore, the transmitter error vector magnitude (EVM) should be lower than −25 dB. In general, the performance of mmWave circuits is strongly related to the semiconductor process. To have a balance between complexity and productivity, complementary metal oxide semiconductor (CMOS) and bipolar CMOS (Bi-CMOS) are the most feasible candidate types, better than more expensive III-V semiconductors, such as GaAs and GaN. Nowadays, the terminated frequency f_t of CMOS and Bi-CMOS transistor is high enough to support the Q-band frequency. The 28-nm CMOS and 130-nm Bi-CMOS can support 300 and 260 GHz, respectively (Rüddenklau et al., 2018). At the moment, semiconductor techniques are not the bottleneck for mmWave RFIC chipsets.

Millimeter-wave transceivers fabricated using either CMOS or Bi-CMOS technology have already been widely researched (Okada, 2019), and can be divided mainly into two kinds of architectures, i.e., direct-conversion and super-heterodyne. Direct-conversion is the simplest way to convert the frequency between an intermediate frequency (IF) signal and mmWave by using an up-mixer and a down-mixer in the transmitter and receiver link, respectively. As for super-heterodyne, the digital baseband counterpart consists of a digital-to-analog converter/analog-to-digital converter (DAC/ADC) and IF mixer, and the frequency conversion between IF and mmWave signals needs to be additionally integrated into the RF beamforming (BF) chip, which is always implemented independently. Furthermore, to support multiple spatial streams, polarization diversity of RF BF chip has been recently studied (Thakkar et al., 2019), and high QAM modulation becomes realistic (Pang et al., 2020) with optimized schematic and layout design of a mmWave transceiver. The design difficulty is reduced for a highly integrated high-performance Q-band transceiver.

Besides the transceiver design, power consumption is another challenge of the mmWave transceiver RFIC, typically with a large number of RF channels, e.g., 64, 128, 256 (Shahramian et al., 2019), or even more. For mmWave RFIC, the power amplifier in the transmitter consumes most of the power for high on-chip loss. According to the power amplifier (PA) survey report (Wang H et al., 2020), as shown in Fig. 3, the peak power-added-efficiency (PAE) and saturated power P_{sat} of CMOS mmWave PA are mainly below 25% and 22 dBm, respectively, similar to those of Bi-CMOS (GeSi). GaAs is a better choice for higher P_{sat}, but it comes with the integration level penalty, resulting in high complexity. When the mmWave PA carries the 64-QAM signal, the average efficiency may be much lower, e.g., less than 5% as reported in Vigilante and Reynaert (2017). Therefore, techniques for efficiency enhancement are considered for application to the mmWave PA, such as (1) supply modulation including envelope tracking (ET) and discrete-level supply bias, (2) load modulation including doherty, outphasing, and load modulated balanced amplifier (LMBA) techniques, (3) mmWave digital pre-distortion (DPD) algorithm, (4) harmonic tuning, and (5) digital power amplifier (DPA).

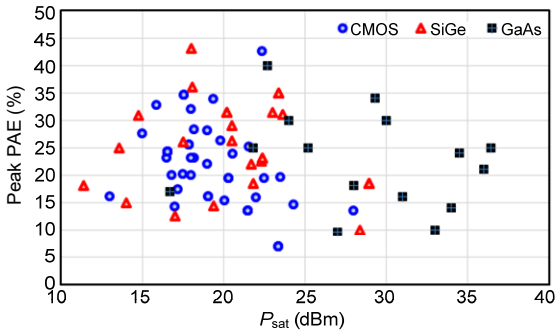

Fig. 3 Peak PAE versus P_{sat} of 40–50 GHz PAs

An ET system has been experimented to improve the efficiency of a Q-band microwave monolithic integrated circuit (MMIC) PA, supporting only 20-MHz signal bandwidth which is much lower than 1080 MHz (Li HT et al., 2019). Doherty and outphasing are the two more promising techniques for high efficiency. These can use the antenna-over-air combining technique to increase the integration level (Wang H et al., 2019). If the Doherty or outphasing architecture is selected, linearization algorithms like DPD are indispensable for supporting high-order QAM modulation (Kelly et al., 2017). Yu C et al. (2020) reported that band-limited DPD can now linearize 800 MHz modulation bandwidth. The harmonic tuning technique (Sarkar and Floyd, 2017) without DPD is another high-efficiency solution for mmWave PA, showing better linearity than load-modulation techniques. DPA operating in switch-mode has been widely researched for the high-efficiency sub-6 GHz transceiver, and now is also introduced to the mmWave transmitter (Deng et al., 2020). As well as the above mentioned circuit-level high-efficiency techniques, system-level energy-efficient methods for the mmWave Internet of Things (IoT) node have been proposed, such as wireless beam modulation (WBM) using the beam propagation information, leading to a low-complexity hardware design (Chen et al., 2020).

The huge propagation loss at the mmWave frequency provides many challenges for real applications. This can be improved by the beamforming technique, in either an analog or digital manner. In the RF analog domain, high performance of the phase shifter is crucial in realizing the beamforming function. State-of-the-art mmWave phase shifters can easily cover an angle range of 360°, while supporting the whole Q-band frequency range, and can also be fabricated using the low-cost CMOS process (Gao and Rebeiz, 2020). Therefore, it is worth further investigating the use of the CMOS process for a Q-band beamforming system.

2.3 Antenna techniques and design

The design of a mmWave antenna has been well researched, including various techniques (Ghosh and Sen, 2019), e.g., metasurface, substrate integrated waveguide (SIW), Fabry–Pérot (FP), antenna-in-package (AiP), and antenna-on-chip (AoC). Because of the small size of a Q-band antenna, the metasurface can be used to enhance performance effectively, including gain, isolation, S11, and 3-dB axis ratio (AR) (Hussain et al., 2020). SIW with low-loss characteristics is quite suitable for mmWave antenna design (Ranjan and Ghosh, 2019), such as for a leaky wave version. FP including a partially reflective surface (PRS) layer is a type of high-gain antenna and can be easily used to achieve beamforming, as recently studied for mmWave, although its multi-layer architecture results in high complexity in fabrication (Emara et al., 2021). AiP is a commercially successful solution for integrating a large antenna array directly with RFIC for a compact mmWave module, but this solution relies strongly on the technology and material of the package (Zhang YP and Mao, 2019). AoC, a more compact antenna solution, directly fabricates the antenna using a chip semiconductor process, but the loss induced by the silicon substrate and the increased complexity because of the larger chip area are the two main shortcomings (Karim et al., 2019).

As to Q-band applications, Wang H and his colleagues (Wang H, 2015; Wang H et al., 2019, 2020) have designed many kinds of antennas using various techniques (Zhang T et al., 2015; Yu SH et al., 2016; Xu et al., 2017; Zhang Y et al., 2017, 2019; Li CF et al., 2019; Liu et al., 2019; Jiang et al., 2020). In Zhang T et al. (2015), a circularly polarized (CP) patch antenna with a simple structure based on a one-layer printed circuit board (PCB) was designed for large 3-dB AR bandwidth, finally reaching 22.8%, i.e., from 37 to 46.5 GHz, while the peak gain is 12.35 dBi. Except the directional high-gain antenna for Q-band AP, Yu SH et al. (2016) reported a wideband omni-directional antenna for Q-band terminals, covering a frequency range from 36 to 50 GHz with 4-dBi gain. In Xu et al. (2017), a Q-band low-profile dual circularly polarized array antenna using the SIW feeding network was designed. This could be used in 2×2 MIMO systems. For wide-angle radiation, a wide-beam Q-band antenna was designed in Zhang Y et al. (2017), successfully covering 120° beamwidth at 45 GHz. In Liu et al. (2019), a tapered slot antenna (TSA) array consisting of eight TSAs was designed to generate the end fire radiation pattern, operating at 42 GHz and reaching 13.9 dBi gain. In Zhang Y et al. (2019), a wideband CP antenna array was also designed with an improved SIW feeding network

including 45°-inclined slot, operating at 45.5 GHz. In Li CF et al. (2019), a CP patch antenna array using a metasurface was proposed, centering at 45 GHz with 32% impedance fractional bandwidth and finally achieving 18.2-dBi peak gain. In Jiang et al. (2020), a low-complexity transmit array supporting multiple beams with only one feed was reported to have high gain (>30 dBi), suggesting its promising use in future Q-band communications systems.

In summary, the design of antennas for Q-band communication is already mature. However, how to integrate it into a single module with RFIC still needs further research for mass production.

2.4 Application outlook

2.4.1 Potential evolution of mmWave components

With the rapid growth of 5G mmWave devices, mmWave components are going to be mature. To balance complexity and performance, a 16-element scale array is a good choice for the Q-band communication system for the home network. In-phase/quadrature (I/Q) direct-conversion transceiver is the simplest architecture for silicon chipset implementation by single frequency conversion, and this is more suitable for Q-band mmWave RFIC design. A digital baseband chipset integrated with ADCs and DACs can be developed independently, using smaller node CMOS technology. A dual polarization antenna array can support more Q-band spatial streams with a smaller size. Also, the AiP technique is very important for compact design. It needs to evaluate multi-beam antenna to support multi-user application. Finally, an intelligent reflection surface (IRS) operating at Q-band would be helpful for enhancing coverage (Perović et al., 2020).

2.4.2 Beamforming in mmWave communication

BF technologies improve mmWave communication capability by focusing the transmitted signal towards the receiver to provide additional link gain (Fig. 4). This can be implemented via full digital BF, full analog BF, and hybrid BF (HBF) (Sun et al., 2014) architectures. For full digital BF systems, each channel consists of individual ADC/DAC and RF chains. Therefore, arbitrary beam steering can be obtained by adjusting phase and amplitude in the digital domain. However, such an architecture is not optimal for mmWave systems with mass channels because of high cost and power consumption. Furthermore, full analog BF is not flexible and the performance is limited. For HBF systems, transmitted signals are first processed through phase shifting in the digital domain and then processed by conventional analog beamformers, thus providing a trade-off between complexity and performance (Kutty and Sen, 2016).

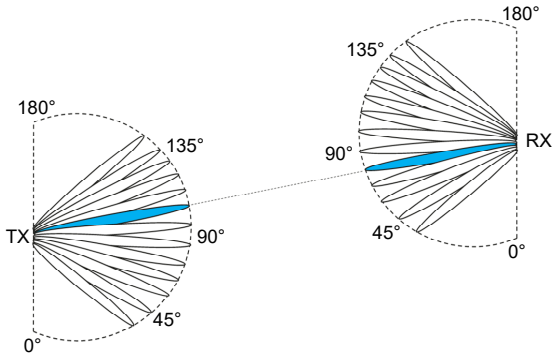

Fig. 4 Beam alignment

Generally, HBF algorithms can be categorized into two types. The first is to take advantages of classical full digital BF technologies to obtain the optimum full digital BF matrix and then the HBF parameters can be obtained by minimizing the Frobenius norm between the HBF matrix and the full digital BF matrix. Typical studies of this type include El Ayach et al. (2014) and Yu XH et al. (2016). Assuming that the channel knowledge is well known at the transmitter, El Ayach et al. (2014) obtained the optimal transmitter and receiver precoding parameters by translating the HBF problem into a sparse reconstruction problem. Nevertheless, perfect channel status (channel state information, CSI) is difficult to obtain in actual scenarios, and thus Zhu et al. (2017) proposed an HBF scheme combined with subspace construction based on limited channel feedback to solve the partial CSI problem. However, for the first type of HBF algorithms, owing to the simplification in regarding the optimization problem as a matrix splitting problem, it usually obtains a sub-optimal result. In contrast, the other type of HBF algorithms regards HBF as a fresh problem and solves the optimization problem directly. This can obtain better results. Typical studies include Sohrabi and Yu (2016) and Lin et al. (2019). AI-based HBF optimizations were also investigated and good results were obtained

(Tao et al., 2020). Multi-beam transmission for a single-user MIMO mode based on HBF was also proposed by Kim et al. (2013), while the guidelines for analysis of optimal streams and spectral efficiency were proposed by Kwon et al. (2014).

HBF for indoor mmWave communication usually consists of three steps (Zhou et al., 2018). First, analog beamforming is trained by beam scanning without considering digital beamforming. Then, the receiver estimates the effective channel and feeds back channel information to the transmitter. Finally, the transmitter calculates the digital beamforming matrix.

For the analog beamforming training, IEEE 802.11aj specifies a selection-based protocol to select the best transmit and receive beam pairs in three phases:

(1) Sector level sweep (SLS): a coarse procedure to decide the best transmit sector and optional receive sector;

(2) Beam refinement phase (BRP): beam refinement training transmit and receive beam pairs with finer beam width;

(3) Beam tracking phase (BT): adjustment of the beam pairs for channel changes in the data transmission stage by appending training fields to data packets.

In this analog beamforming training, codebook design and efficient beam alignment are two important problems. For codebook design, complexity and protocol overheads attracted much attention (Kutty and Sen, 2016). For beam alignment (BA), search complexity is determined by the number of training symbols required to select the beam pair with the highest signal-to-noise ratio (SNR). The most straightforward beam alignment is exhaustive search, in which the transmitter and receiver scan all the beam pairs and find the strong beam pairs (Akdeniz et al., 2014). To decrease time consumption, several optimization methods have been proposed. These algorithms are all aimed at achieving reliable beam alignment using less overhead than exhaustive search. Palacios et al. (2017) proposed a two-stage pseudo-exhaustive beam alignment scheme. The key point is to do a coarse beam alignment first and then conduct a mode-refined BA. Similar research can be found in Noh et al. (2017). Moreover, the nature of mmWave channels, i.e., the sparse attribution in the beam domain, motivates studies to introduce compressed sensing (Rodríguez-Fernández et al., 2018) to improve BA. The compressed sensing-based methods show particularly attractive improvements for the multi-user environment but suffer from low SNR. In addition, WiFi-positioning-based beam alignment algorithms (Mubarak et al., 2016) were used to reduce the searching codebook. Tsang et al. (2011) also used a beam coding mechanism to enable multiple beams to steer simultaneously in BF training.

After analog BF, the possible analog beam pairs will be obtained and can be used to calculate digital BF parameters (Zhou et al., 2018). In the digital BF training, multiple beam pairs will all be tried and the best transmit-receive beam combinations can be determined (Ghasempour et al., 2017). The algorithm for determining the best beam pairs is implementation-dependent. For the FTTR scenario, the requirement for beam alignment could be simplified because the coverage area is usually limited to a single room and wide beam can also be useful. Furthermore, requirements for HBF methods can be simplified when the spectrum resource is almost infinite and could support an ultra-high data rate for isolated rooms.

2.4.3 Roaming in the mmWave network

Currently, the multi-AP solution is quite successful in the market for bringing better signal coverage. In this case, roaming is an indispensable feature for seamless connection. As Fig. 5 shows, classical WiFi roaming typically contains the following steps:

(1) Station (STA) identifies low-quality signal environments by the received signal strength indicator (RSSI), bit error rate (BER), or other related physical layer parameters;

(2) WiFi AP works with STA to change the connection to an alternative AP by a roaming protocol such as 802.11k (IEEE, 2008a);

(3) Current connecting AP informs STA to switch to the selected AP by 802.11v (IEEE, 2011) and 802.11r (IEEE, 2008b) to improve the handover efficiency. Authentication, association, and encryption related procedures are completed in this step.

However, it is difficult for mmWave to use the roaming procedure above. Because Q-band mmWave communication is usually based on line-of-sight (LoS), it is challenging for an AP in this band to sense the existence of other APs with significant building

blockage between each other. It is necessary to develop a new strategy. For example, centralized management and control by an agile controller (AC) server can be used to distribute mmWave APs. In the FTTR architecture, each AP connects to the optical network terminal of the access network through fiber. In this scenario, roaming can be controlled in a centralized way. Furthermore, to enhance coverage and stability of handover between mmWave APs, multiple links based on multiple beams or multiple bands are also proposed. For example, low-frequency channels (2.4 GHz) can be used as stable connections to transfer management messages to avoid reassociation processes including beam alignment when handover between mmWave APs occurs. Clearly, mmWave device roaming has many distinct features and needs further research when compared to classical WiFi technology.

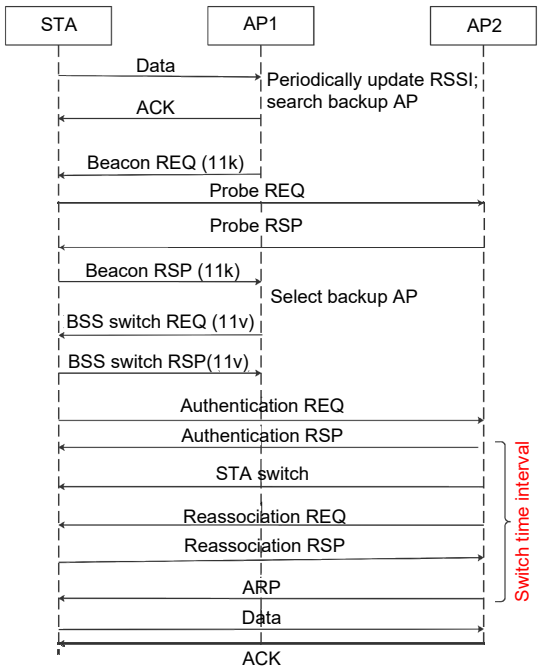

Fig. 5 Typical AP switching procedures (IEEE, 2008a, 2008b, 2011)

3 Commercialization of Q-band products

3.1 Cloud VR and relevant network requirement for a home network

Cloud VR makes use of cloud computing and cloud rendering for VR services. With fast and stable networks, cloud-based audiovisual contents are coded, compressed, and transmitted to end user devices, delivering cloud-based VR services (Zhang XZ et al., 2019).

In general, cloud VR places strict requirements on the network bearer. It can be transported together with current Internet services. However, in that case, these services are packaged and streamlined for transmission with strong coupling and competition between each other. It is difficult to guarantee the VR service experience because of the current IP forwarding network without slicing. To ensure an excellent VR experience, it is better to transport VR traffic through an independent channel separated from existing Internet services (ETSI F5G Industrial Specification Group, 2021). To implement this, the ONT needs to recognize cloud VR traffic and direct it to corresponding sliced channels, along with providing quality-of-service (QoS) guaranteed resources. The concept is shown in Fig. 6.

The characteristics and corresponding network requirements are summarized in Table 3 (Zhang XZ et al., 2019), which shows that one ultimate VR streaming requires multiple Gb/s guaranteed data rate and only a few milliseconds latency budget in a home network.

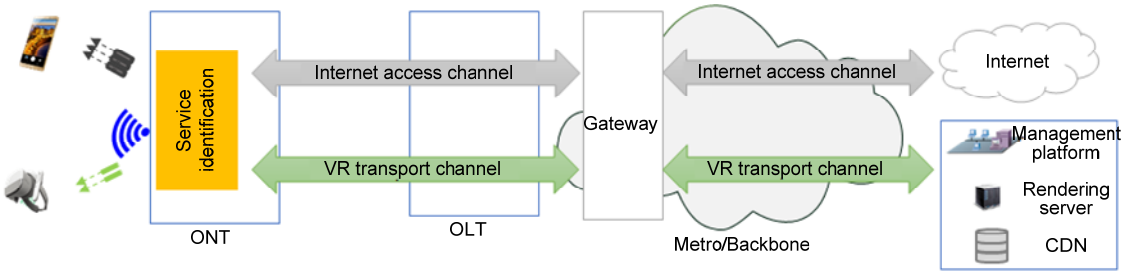

Fig. 6 Schematic of the architecture for FTTR (ETSI F5G Industrial Specification Group, 2021)

ONT: optical network terminal; OLT: optical line terminal; VR: virtual reality; CDN: content delivery network

Table 3 Network requirements of could VR

VR	Data rate (Mb/s)		RTT (ms)		Packet loss rate ($\times10^{-6}$)		Full-view resolution of video
	VR online video	VR cloud gaming	VR online video	VR cloud gaming	VR online video	VR cloud gaming	
Pre-VR	25	50	30	20	240	10	4K 2D: 3840×1920
Elementary VR	75 (2D); 120 (3D)	150 (2D); 250 (3D)	30 (2D); 20 (3D)	10	24	1.0	8K 2D/3D: 7680×3840
Advanced VR	630	1.4×1024	20	5	1.0	1.0	12K 3D: 11 520×5760
Ultimate VR	4.40×1024	3.36×1024	10	5	1.0	1.0	24K 3D: 23 040×11 520

Current WiFi technology (e.g., 802.11ax) operating at 2.4 and 5 GHz finds it difficult to satisfy the requirements of cloud VR in many scenarios because of limited spectrum, neighbor interference usage, and a collision-based protocol. Fortunately, mmWave has the following advantages to solve these challenges:

(1) There is an additional 100 dB loss in penetrating a concrete wall as shown in Fig. 7, to provide high isolation among rooms.

(2) The current mmWave protocol IEEE 802.11aj uses the time-division multiplexing (TDM) mode in the MAC layer, avoiding potential collision due to competing with the air interface.

(3) The Q-band with 6-GHz bandwidth (Fig. 8), which is about 10 times wider than the existing 802.11ax spectrum, was released in 2013 from 42 to 48 GHz, in China.

However, with all these advantages, widely deploying mmWave devices still involves the need to solve practical issues.

In the common fiber-to-the-home (FTTH) solution of China, the ONT is put in the information box which normally is metal or plastic sheathed and locates near the entrance of an apartment. The environment of the information box limits the use of the mmWave directly from the ONT since larger attenuation will take place in going through the information box and nearby walls. Another approach is to make use of existing copper media (including phone line, coaxial cable, or power line) as backhaul links for mmWave products. However, these backhaul links are at a low data rate because of larger attenuation fading channels. New backhauling needs to be developed to make best use of mmWave capabilities.

Service requires high data rate. Current network services, such as audio, HD/4K video, web browsing, and file downloading, need a data rate of less than 100 Mb/s. Conventional WiFi technology has met the needs of such services. With the deployment of cloud VR, there are new opportunities for mmWave.

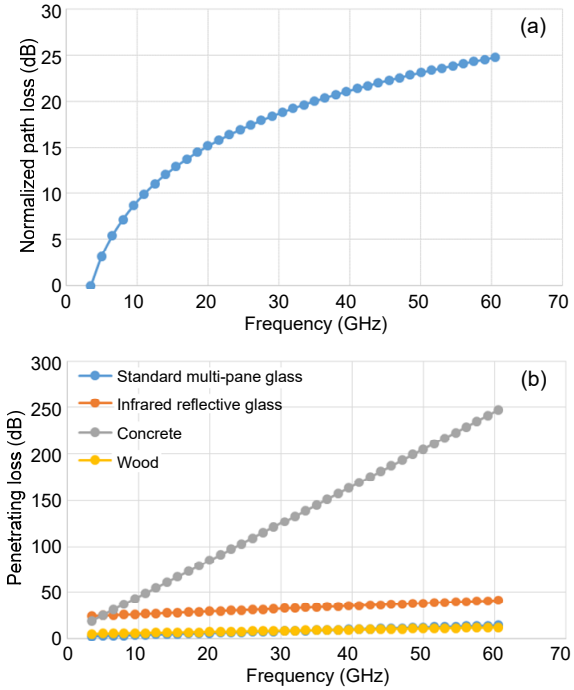

Fig. 7 Signal loss over different radio frequencies: (a) path loss of different RF signals; (b) penetrating loss for different media (References to color refer to the online version of this figure)

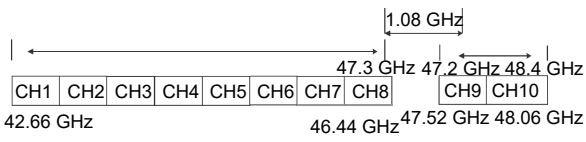

Fig. 8 Q-band spectrum released in 2013 by the Chinese government

The current fiber access network is evolving from GPON to 10G-PON, bringing the upgrade of the access network to the Gb/s era. In this new era, the transport and access network outside apartments will no longer be the bottleneck of data rate limits.

3.2 Fiber as mmWave backhaul

As discussed in Section 1, in 2019, ETSI established a new ISG F5G to define the fifth generation of the fixed network. F5G considers the migration of the reference architecture from FTTH to FTTR.

FTTR is created to provide an extremely high broadband with perfect coverage everywhere within the home. Currently, WiFi is the main technology widely deployed to provide the last 10-m connection to end users. With the increasing demand of network throughput from various services, and to solve the wall penetration loss problem, a multi-AP solution is used to improve the signal coverage within the home, practically realizing similar signal strength almost everywhere. By using wireless backhaul, spectrum resources may be shared between backhaul and fronthaul, or more RF links need to be used. These solutions will either reduce the connection broadband bandwidth or increase product complexity. In addition, the collision probability over air interfaces will get worse due to the limited RF spectrum, leading to performance degradation in terms of data rate, latency, and stability. To ideally solve the backhaul problem, fiber is the best choice since the modulation bandwidth is nearly unlimited compared to any other wired metallic medium. Under the new architecture of FTTR, backhaul connection for new services (e.g., cloud VR/AR and holograms that require tens of Gb/s and less than millisecond latency) is no longer a bottleneck. To replace the current WiFi unqualified connection, mmWave based on Q-band is a promising approach to guarantee the required data rate and latency in those advanced multimedia applications.

3.3 Indoor channel modeling

To further optimize communication capability using mmWave technology, it is necessary to adapt the system to mmWave indoor transmission models. Channel models are commonly classified into two types, known as analytical and physical models. Analytical models are usually based on mathematical analysis of the channel, while physical models are described on the basis of their electronic wave propagation characteristics. Usually, the analytical models can be derived from the physical models, so we focus on the physical models of millimeter channels here. For physical channel models, they are divided into deterministic and stochastic. Ray-tracing (RT) techniques, which are best suited for deterministic models, are widely used to describe mmWave channels to simulate a desired channel scenario. Furthermore, RT can predict new environmental characteristics. Several studies based on RT have been conducted to describe the propagation characteristics in different mmWave scenarios (Alexander et al., 2010; Hemadeh et al., 2017). Fig. 9 (IEEE, 2010) shows an example for modeling the channel of a living room. Possible transportation routes are illustrated. In general, LoS and non-light-of-sight (NLoS) are used to describe the channel condition. LoS indicates no blockage between the transmitter and the receiver, therefore leading to minimum loss of signal. When LoS is not available because of blockage, a transmission link can be established through NLoS links, such as reflection or refraction. The lower part in Fig. 9 demonstrates possible reflection routes (1^{st} order and 2^{nd} order) that can be used for signal transmission. In this case, the signal suffers from larger transmission attenuation because of longer transmission routes and additional reflection loss.

In contrast to deterministic models, stochastic models (Cui et al., 2019) describe the spatial-temporal characteristics of the channel by impulse response according to many measurements from real environments. The probability density functions of channel characteristics are used for describing large- and small-scale fading features. Stochastic channel models are considered simple and thus reduce the complexity for system design and simulation. Several mmWave channel models have been developed in recent years for indoor communication scenarios (Table 4). For a detailed comparison of these models, please refer to Hemadeh et al. (2017).

4 Prototype measurements

He et al. (2017) developed a mmWave prototype, achieving 4 Gb/s data rate. In this section, we demonstrate a Q-band prototype with 4-port

Table 4 mmWave channel models (Hemadeh et al., 2017)

Technology	Frequency	Year	Channel model	Description
WPAN	60 GHz	2007	TG3c	Proposing a channel model for 60 GHz, where nine scenarios with both NLoS and LoS environments are identified
WLAN	60 GHz	2010	TGad	Statistical models of the indoor 60 GHz channel; BF considered
WLAN	60 GHz	2014	Cluster double directional model	Measurements based channel model
Indoor	45 GHz	2015	Hybrid channel model	Hybrid 45 GHz model for indoor conference room; based on both measurements and RT
Indoor	60 GHz	2015	Statistical channel model	Based on spatial-temporal indoor measurements

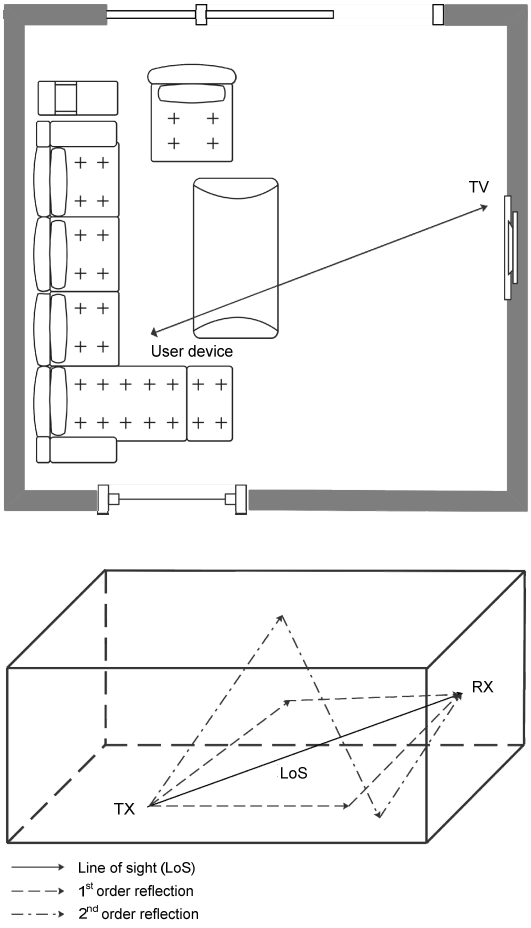

Fig. 9 Ray tracing model for mmWave transmission in a living room (IEEE, 2010)

transmission and reception capability. As shown in Fig. 10, the system consists of three parts: a digital front end (DFE), an analog front end (AFE), and a radio frequency (RF) module. The implementation is based on the 802.11aj protocol. The 1080-MHz channel bandwidth and 16-QAM modulation are supported. Fig. 11 shows the RF test bed, including an

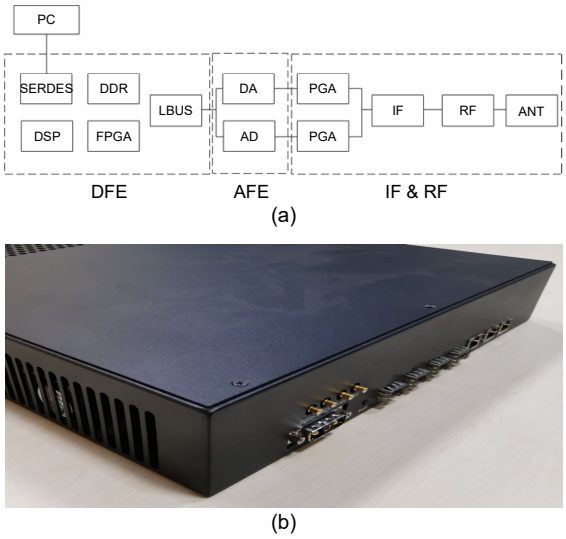

Fig. 10 Q-band prototype: (a) prototype blocks; (b) prototype appearance

R&S vector signal generator SMW200A to generate 802.11aj signals and a signal spectrum analyzer FSW to measure signal quality in the baseband and RF band. Fig. 12 shows the transmitting intermediate frequency (IF) signal at 3 GHz, while the actual bandwidth is 1.1 GHz when the symbol rate is set to 1 Gsym/s with single carrier modulation. From envelopes of the signal and noise, the SNR is estimated to be approximately 33 dB.

To measure the loopback performance from transmitter to receiver, experiments using wireline cable to connect the transmitter and receiver directly are conducted. As Fig. 13 shows, SNRs of 25 and 20 dB are obtained in the channel bandwidths of 540 MHz (Figs. 13a and 13b) and 1080 MHz (Figs. 13c and 13d), respectively. Up to 2 Gb/s per stream is achieved with 16-QAM modulation and a total data rate up to 8 Gb/s can be reached.

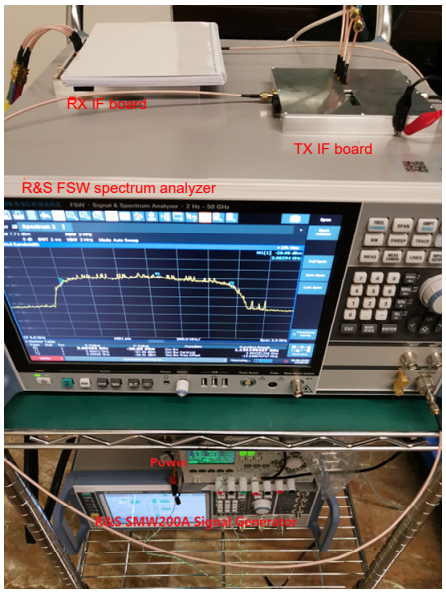

Fig. 11 Test bed for Q-band RF modules

5 Conclusions

The main contribution of this paper is to propose a novel home network architecture: Q-band mmWave communication over FTTR. This is a promising solution to the next generation home networks, compared

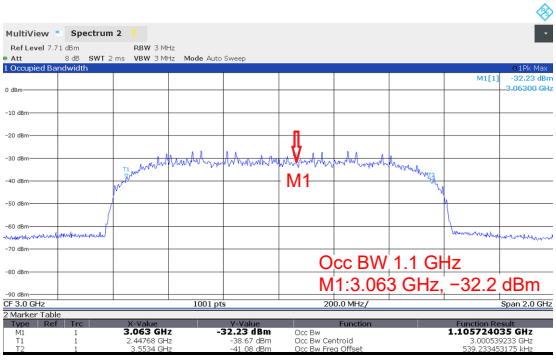

Fig. 12 Transmitting IF signals

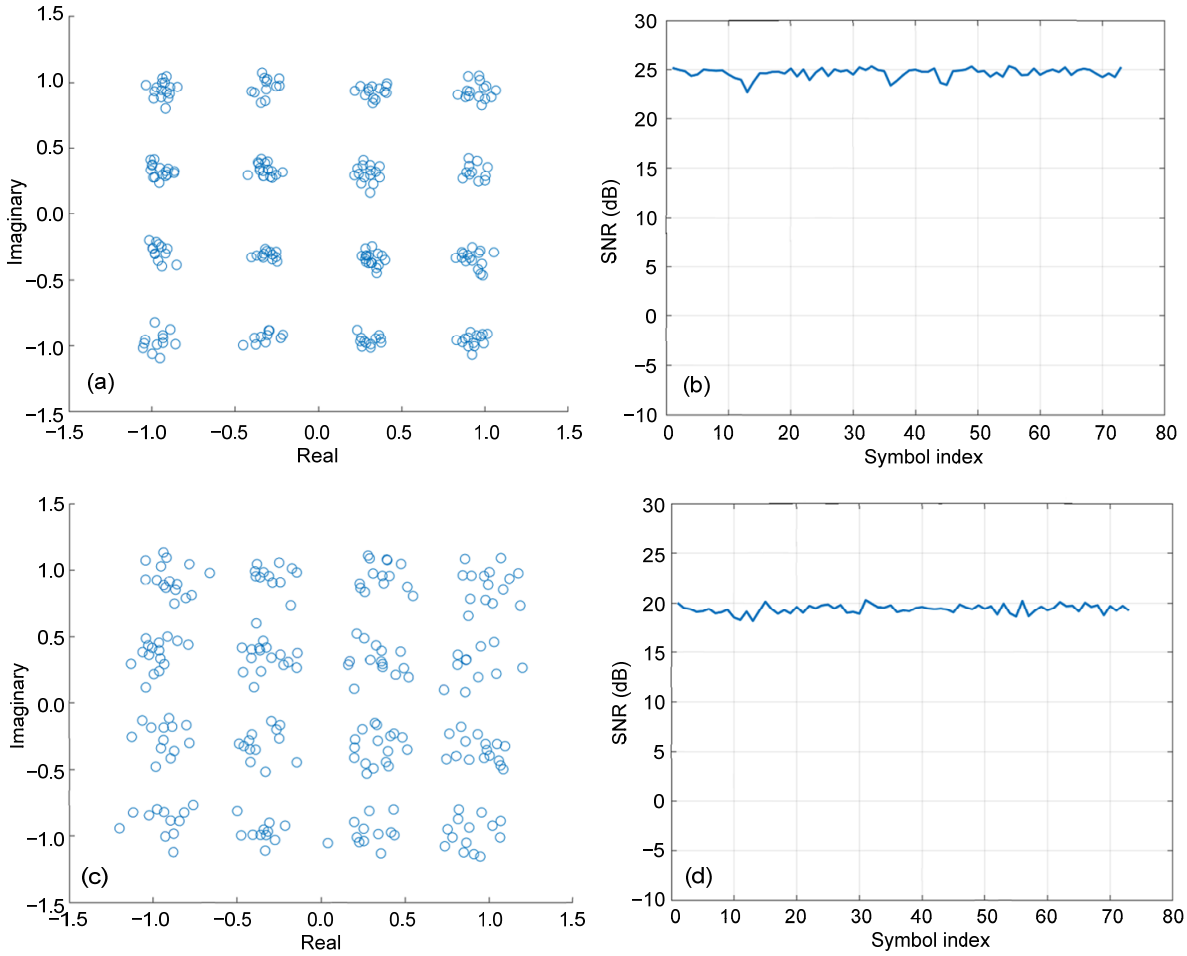

Fig. 13 Loopback measurement results: (a) constellation mapping of 540 MHz profile; (b) SNR of each symbol for 540 MHz profile; (c) constellation mapping of 1080 MHz profile; (d) SNR of each symbol for 1080 MHz profile

with other candidate solutions (including mesh WiFi and WiFi over wired G.hn (ITU-T, 2020c)). This novel solution can guarantee that the QoS of a home network will be suitable for advanced emerging cloud VR/AR and hologram services. FTTR provides nearly unlimited backhaul throughput using a fiber connection, while Q-band mmWave provides an extremely high data rate and avoids interference under a shared unlicensed band.

There have been many studies on how to better design Q-band mmWave transmission systems to support future advanced home network services, e.g., how to effectively improve Q-band performance by using massive MIMO, beamforming, roaming, and advanced IF/RF and antenna design. However, efficient protocols and system level integration need to be thoroughly investigated. For the prototype shown in Section 4, more efforts need to be made to evaluate and verify the in-home use cases.

Standardization efforts are also necessary for the industry ecosystem to conduct mass production and deployment. New non-communication applications (e.g., positioning, detection, health-care, and home security) may be developed on top of the communication system. Moreover, openness of the Q-band spectrum for indoor usage needs further consideration in spectrum regulation in ITU-R.

Contributors

Xiang WANG proposed the concept and supervised the research. Xiang WANG, Yan ZENG, Zhixiong REN, and Chao HE processed the data and drafted the manuscript. Jian FANG, Debin HOU, and Zhe CHEN helped organize the manuscript. Le KUAI, Rong LU, Shilin YANG, Zhe CHEN, and Jixin CHEN conducted the experiments and validation. Chao HE, Yan ZENG, and Zhixiong REN revised and finalized the paper.

Acknowledgements

The authors would like to acknowledge Prof. Wei HONG and his team at Southeast University, Dejian LI and Jiamin CHEN at Huawei Technologies, for their valuable advice.

Compliance with ethics guidelines

Chao HE, Zhixiong REN, Xiang WANG, Yan ZENG, Jian FANG, Debin HOU, Le KUAI, Rong LU, Shilin YANG, Zhe CHEN, and Jixin CHEN declare that they have no conflict of interest.

References

Ai B, Guan K, He RS, et al., 2017. On indoor millimeter wave massive MIMO channels: measurement and simulation. *IEEE J Sel Areas Commun*, 35(7):1678-1690. https://doi.org/10.1109/JSAC.2017.2698780

Akdeniz MR, Liu YP, Samimi MK, et al., 2014. Millimeter wave channel modeling and cellular capacity evaluation. *IEEE J Sel Areas Commun*, 32(6):1164-1179. https://doi.org/10.1109/JSAC.2014.2328154

Alexander M, Vinko E, Chris H, et al., 2010. Channel Models for 60 GHz WLAN Systems. No. 11-09-0334-08, IEEE 802.11.

Alkhateeb A, El Ayach O, Leus G, et al., 2014. Channel estimation and hybrid precoding for millimeter wave cellular systems. *IEEE J Sel Top Signal Process*, 8(5):831-846. https://doi.org/10.1109/JSTSP.2014.2334278

Chen JN, Li S, Tao JY, et al., 2020. Wireless beam modulation: an energy- and spectrum-efficient communication technology for future massive IoT systems. *IEEE Wirel Commun*, 27(5):60-66. https://doi.org/10.1109/MWC.001.2000021

Cui PF, Zhang JA, Lu WJ, et al., 2019. Statistical sparse channel modeling for measured and simulated wireless temporal channels. *IEEE Trans Wirel Commun*, 18(12): 5868-5881. https://doi.org/10.1109/TWC.2019.2940017

Deng W, Song Z, Ma RC, et al., 2020. An energy-efficient 10-Gb/s CMOS millimeter-wave transceiver with direct-modulation digital transmitter and I/Q phase-coupled frequency synthesizer. *IEEE J Sol-State Circ*, 55(8): 2027-2042. https://doi.org/10.1109/JSSC.2020.2978022

El Ayach O, Rajagopal S, Abu-Surra S, et al., 2014. Spatially sparse precoding in millimeter wave MIMO systems. *IEEE Trans Wirel Commun*, 13(3):1499-1513. https://doi.org/10.1109/TWC.2014.011714.130846

Emara MK, Tomura T, Hirokawa J, et al., 2021. All-dielectric Fabry-Pérot-based compound Huygens' structure for millimeter-wave beamforming. *IEEE Trans Antenn Propag*, 69(1):273-285. https://doi.org/10.1109/TAP.2020.3005233

ETSI, 2019. Terms of Reference (ToR) for ETSI ISG "5th Generation Fixed Network" (ISG F5G). European Tele-Communications Standards Institute, Nice, France.

ETSI F5G Industrial Specification Group, 2021. Fifth Generation Fixed Network (F5G): F5G Use Cases Release. ETSI GR F5G-002.

Gao L, Rebeiz GM, 2020. A 22–44-GHz phased-array receive beamformer in 45-nm CMOS SOI for 5G applications with 3–3.6-dB NF. *IEEE Trans Microw Theory Techn*, 68(11):4765-4774. https://doi.org/10.1109/TMTT.2020.3004820

Genc Z, Dang BL, Wang J, et al., 2008. Home networking at 60 GHz: challenges and research issues. *Ann Telecommun*, 63(9):501-509. https://doi.org/10.1007/s12243-008-0047-0

Ghasempour Y, Da Silva CRCM, Cordeiro C, et al., 2017. IEEE 802.11ay: next-generation 60 GHz communication for 100 Gb/s Wi-Fi. *IEEE Commun Mag*, 55(12):186-192. https://doi.org/10.1109/MCOM.2017.1700393

Ghosh S, Sen D, 2019. An inclusive survey on array antenna

design for millimeter-wave communications. *IEEE Access*, 7:83137-83161. https://doi.org/10.1109/ACCESS.2019.2924805

Guillory J, Tanguy E, Pizzinat A, et al., 2011. A 60 GHz wireless home area network with radio over fiber repeaters. *J Lightw Technol*, 29(16):2482-2488. https://doi.org/10.1109/JLT.2011.2159776

He SW, Huang YM, Wang HM, et al., 2017. Development trend and technological challenges of millimeter-wave wireless communication. *Telecommun Sci*, 33(6):11-20 (in Chinese). https://doi.org/10.11959/j.issn.1000-0801.2017202

Hemadeh IA, Satyanarayana K, El-Hajjar M, et al., 2017. Millimeter-wave communications: physical channel models, design considerations, antenna constructions, and link-budget. *IEEE Commun Surv Tutor*, 20(2):870-913. https://doi.org/10.1109/COMST.2017.2783541

Hirata A, Kosugi T, Takahashi H, et al., 2006. 120-GHz-band millimeter-wave photonic wireless link for 10-Gb/s data transmission. *IEEE Trans Microw Theory Techn*, 54(5): 1937-1944. https://doi.org/10.1109/TMTT.2006.872798

Hur S, Kim T, Love DJ, et al., 2013. Millimeter wave beamforming for wireless backhaul and access in small cell networks. *IEEE Trans Commun*, 61(10):4391-4403. https://doi.org/10.1109/TCOMM.2013.090513.120848

Hussain N, Jeong MJ, Abbas A, et al., 2020. A metasurface-based low-profile wideband circularly polarized patch antenna for 5G millimeter-wave systems. *IEEE Access*, 8:22127-22135. https://doi.org/10.1109/ACCESS.2020.2969964

IEEE, 2008a. IEEE Standard for Information Technology—Local and Metropolitan Area Networks—Specific Requirements—Part 11: Wireless LAN Medium Access Control (MAC) and Physical Layer (PHY) Specifications Amendment 1: Radio Resource Measurement of Wireless LANs, IEEE 802.11k-2008. National Standards of the United States of America. https://doi.org/10.1109/IEEESTD.2008.4544755

IEEE, 2008b. IEEE Standard for Information Technology—Local and Metropolitan Area Networks—Specific Requirements—Part 11: Wireless LAN Medium Access Control (MAC) and Physical Layer (PHY) Specifications Amendment 2: Fast Basic Service Set (BSS) Transition, 802.11r-2008. National Standards of the United States of America. https://doi.org/10.1109/IEEESTD.2008.4573292

IEEE, 2009. IEEE Standard for Information Technology—Local and Metropolitan Area Networks—Specific Requirements—Part 15.3: Amendment 2: Millimeter-Wave-Based Alternative Physical Layer Extension, 802.15.3c-2009. National Standards of the United States of America. https://doi.org/10.1109/IEEESTD.2009.5284444

IEEE, 2010. Citing Electronic Sources of Information. https://mentor.ieee.org/802.11/dcn/09/11-09-0334-08-00ad-channel-models-for-60-ghz-wlan-systems.doc

IEEE, 2011. IEEE Standard for Information Technology—Local and Metropolitan Area Networks—Specific Requirements—Part 11: Wireless LAN Medium Access Control (MAC) and Physical Layer (PHY) Specifications Amendment 8: IEEE 802.11 Wireless Network Management, 802.11v-2011. National Standards of the United States of America. https://doi.org/10.1109/10.1109/IEEESTD.2011.5716530

IEEE, 2012. IEEE Standard for Information Technology—Telecommunications and Information Exchange Between Systems—Local and Metropolitan Area Networks—Specific Requirements—Part 11: Wireless LAN Medium Access Control (MAC) and Physical Layer (PHY) Specifications Amendment 3: Enhancements for Very High Throughput in the 60 GHz Band, 802.11ad-2012. National Standards of the United States of America. https://doi.org/10.1109/IEEESTD.2012.6392842

IEEE, 2018. IEEE Standard for Information Technology—Telecommunications and Information Exchange Between Systems—Local and Metropolitan Area Networks—Specific Requirements—Part 11: Wireless LAN Medium Access Control (MAC) and Physical Layer (PHY) Specifications Amendment 3: Enhancements for Very High Throughput to Support Chinese Millimeter Wave Frequency Bands (60 GHz and 45 GHz), 802.11aj-2018. National Standards of the United States of America. https://doi.org/10.1109/IEEESTD.2018.8345727

ITU-T, 1999. Asymmetric Digital Subscriber Line (ADSL) Transceivers. ITU-T G.992.1, International Telecommunication Union, Geneva.

ITU-T, 2008. Gigabit-Capable Passive Optical Networks (GPON): General Characteristics. ITU-T G.984.1, International Telecommunication Union, Geneva.

ITU-T, 2009. Unified High-Speed Wireline-Based Home Networking Transceivers—System Architecture and Physical Layer Specification. ITU-T G.9960, International Telecommunication Union, Geneva.

ITU-T, 2016. 10-Gigabit-Capable Passive Optical Networks (XG-PON): General Requirements. ITU-T G.987.1, International Telecommunication Union, Geneva.

ITU-T, 2019a. Fast Access to Subscriber Terminals (G.fast)—Physical Layer Specification. ITU-T G.9701, International Telecommunication Union, Geneva.

ITU-T, 2019b. Higher Speed Passive Optical Networks—Requirements. ITU-T G.9804.1, International Telecommunication Union, Geneva.

ITU-T, 2019c. Very High Speed Digital Subscriber Line Transceivers 2 (VDSL2). ITU-T G.993.2, International Telecommunication Union, Geneva.

ITU-T, 2020a. Multi-Gigabit Fast Access to Subscriber Terminals (MGfast)—Power Spectral Density Specification. ITU-T G.9710, International Telecommunication Union, Geneva.

ITU-T, 2020b. SG15-TD465R1/PLEN, WP1/15 Meeting Report. International Telecommunication Union, Geneva.

ITU-T, 2020c. SG15-TD468/WP1, G.9960-2 (G.hn Evolution):

Draft Text. International Telecommunication Union, Geneva.

Jiang ZH, Kang L, Yue TW, et al., 2020. Wideband transmit arrays based on anisotropic impedance surfaces for circularly polarized single-feed multibeam generation in the Q-band. *IEEE Trans Antenn Propag*, 68(1):217-229. https://doi.org/10.1109/TAP.2019.2943343

Karim R, Iftikhar A, Ijaz B, et al., 2019. The potentials, challenges, and future directions of on-chip-antennas for emerging wireless applications—a comprehensive survey. *IEEE Access*, 7:173897-173934. https://doi.org/10.1109/ACCESS.2019.2957073

Kelly N, Cao WH, Zhu AD, 2017. Preparing linearity and efficiency for 5G: digital predistortion for dual-band Doherty power amplifiers with mixed-mode carrier aggregation. *IEEE Microw Mag*, 18(1):76-84. https://doi.org/10.1109/MMM.2016.2616185

Kim C, Kim T, Seol JY, 2013. Multi-beam transmission diversity with hybrid beamforming for MIMO-OFDM systems. Proc IEEE Globecom Workshops, p.61-65. https://doi.org/10.1109/GLOCOMW.2013.6824962

Kutty S, Sen D, 2016. Beamforming for millimeter wave communications: an inclusive survey. *IEEE Commun Surv Tutor*, 18(2):949-973. https://doi.org/10.1109/COMST.2015.2504600

Kwon G, Shim Y, Park H, et al., 2014. Design of millimeter wave hybrid beamforming systems. Proc IEEE 80th Vehicular Technology Conf, p.1-5. https://doi.org/10.1109/VTCFall.2014.6965933

Li CF, Zhu XW, Liu PF, et al., 2019. A metasurface-based multilayer wideband circularly polarized patch antenna array with a parallel feeding network for Q-band. *IEEE Antenn Wirel Propag Lett*, 18(6):1208-1212. https://doi.org/10.1109/LAWP.2019.2912624

Li HT, Zhu XW, Zhong NY, et al., 2019. A 20MHz supply modulator designed for envelope tracking power amplifier at 42GHz. Proc Int Conf on Microwave and Millimeter Wave Technology, p.1-3. https://doi.org/10.1109/ICMMT45702.2019.8992149

Lin T, Cong JQ, Zhu Y, et al., 2019. Hybrid beamforming for millimeter wave systems using the MMSE criterion. *IEEE Trans Commun*, 67(5):3693-3708. https://doi.org/10.1109/TCOMM.2019.2893632

Liu PF, Zhu XW, Jiang ZH, et al., 2019. A compact single-layer Q-band tapered slot antenna array with phase-shifting inductive windows for endfire patterns. *IEEE Trans Antenn Propag*, 67(1):169-178. https://doi.org/10.1109/TAP.2018.2876727

Marcus M, Pattan B, 2005. Millimeter wave propagation: spectrum management implications. *IEEE Microw Mag*, 6(2):54-62. https://doi.org/10.1109/MMW.2005.1491267

MIIT, 2013. The Usage of 40–50 GHz Frequency Band for Mobile Services in Broadband Wireless Access Systems.

Moraitis N, Constantinou P, 2004. Indoor channel measurements and characterization at 60 GHz for wireless local area network applications. *IEEE Trans Antenn Propag*, 52(12):3180-3189. https://doi.org/10.1109/TAP.2004.836422

Mubarak ASA, Mohamed EM, Esmaiel H, 2016. Millimeter wave beamforming training, discovery and association using WiFi positioning in outdoor urban environment. Proc 28th Int Conf on Microelectronics, p.221-224. https://doi.org/10.1109/ICM.2016.7847855

Noh S, Zoltowski MD, Love DJ, 2017. Multi-resolution codebook and adaptive beamforming sequence design for millimeter wave beam alignment. *IEEE Trans Wirel Commun*, 16(9):5689-5701. https://doi.org/10.1109/TWC.2017.2713357

Okada K, 2019. Millimeter-wave phased-array transceiver using CMOS technology. Proc IEEE Asia-Pacific Microwave Conf, p.729-731. https://doi.org/10.1109/APMC46564.2019.9038302

Palacios J, de Donno D, Widmer J, 2017. Tracking mm-Wave channel dynamics: fast beam training strategies under mobility. Proc IEEE Conf on Computer Communications, p.1-9. https://doi.org/10.1109/INFOCOM.2017.8056991

Pang J, Li Z, Kubozoe R, et al., 2020. A 28-GHz CMOS phased-array beamformer utilizing neutralized bi-directional technique supporting dual-polarized MIMO for 5G NR. *IEEE J Sol-State Circ*, 55(9):2371-2386. https://doi.org/10.1109/JSSC.2020.2995039

Perović NS, di Renzo M, Flanagan MF, 2020. Channel capacity optimization using reconfigurable intelligent surfaces in indoor mmWave environments. Proc IEEE Int Conf on Communications, p.1-7. https://doi.org/10.1109/ICC40277.2020.9148781

Rangan S, Rappaport TS, Erkip E, 2014. Millimeter-wave cellular wireless networks: potentials and challenges. *Proc IEEE*, 102(3):366-385. https://doi.org/10.1109/JPROC.2014.2299397

Ranjan R, Ghosh J, 2019. SIW-based leaky-wave antenna supporting wide range of beam scanning through broadside. *IEEE Antenn Wirel Propag Lett*, 18(4):606-610. https://doi.org/10.1109/LAWP.2019.2897836

Rodríguez-Fernández J, González-Prelcic N, Venugopal K, et al., 2018. Frequency-domain compressive channel estimation for frequency-selective hybrid millimeter wave MIMO systems. *IEEE Trans Wirel Commun*, 17(5):2946-2960. https://doi.org/10.1109/TWC.2018.2804943

Rüddenklau U, Geen M, Andrea P, et al., 2018. mmWave Semiconductor Industry Technologies: Status and Evolution. ETSI White Paper No. 15, ETSI, p.1-53. https://www.etsi.org/images/files/ETSIWhitePapers/etsi_wp15ed2_mmWave-Semiconductor_Technologies_FINAL.pdf

Sarkar A, Floyd BA, 2017. A 28-GHz harmonic-tuned power amplifier in 130-nm SiGe BiCMOS. *IEEE Trans Microw Theory Techn*, 65(2):522-535. https://doi.org/10.1109/TMTT.2016.2636842

Sato K, Manabe T, Ihara T, et al., 1997. Measurements of reflection and transmission characteristics of interior structures of office building in the 60-GHz band. *IEEE*

Trans Antenn Propag, 45(12):1783-1792. https://doi.org/10.1109/8.650196

Shahramian S, Holyoak MJ, Singh A, et al., 2019. A fully integrated 384-element, 16-tile, *W*-band phased array with self-alignment and self-test. *IEEE J Sol-State Circ*, 54(9):2419-2434. https://doi.org/10.1109/JSSC.2019.2928694

Sohrabi F, Yu W, 2016. Hybrid digital and analog beamforming design for large-scale antenna arrays. *IEEE J Sel Top Signal Process*, 10(3):501-513. https://doi.org/10.1109/JSTSP.2016.2520912

Sun S, Rappaport TS, Heath RW, et al., 2014. MIMO for millimeter-wave wireless communications: beamforming, spatial multiplexing, or both? *IEEE Commun Mag*, 52(12): 110-121. https://doi.org/10.1109/MCOM.2014.6979962

Tao JY, Chen JN, Xing J, et al., 2020. Autoencoder neural network based intelligent hybrid beamforming design for mmWave massive MIMO systems. *IEEE Trans Cogn Commun Netw*, 6(3):1019-1030. https://doi.org/10.1109/TCCN.2020.2991878

Thakkar C, Chakrabarti A, Yamada S, et al., 2019. A 42.2-Gb/s 4.3-pJ/b 60-GHz digital transmitter with 12-b/symbol polarization MIMO. *IEEE J Sol-State Circ*, 54(12):3565-3576. https://doi.org/10.1109/JSSC.2019.2943924

Tsang YM, Poon ASY, Addepalli S, 2011. Coding the beams: improving beamforming training in mmWave communication system. Proc IEEE Global Telecommunications Conf, p.1-6. https://doi.org/10.1109/GLOCOM.2011.6134486

Vigilante M, Reynaert P, 2017. A 29-to-57GHz AM-PM compensated class-AB power amplifier for 5G phased arrays in 0.9V 28nm bulk CMOS. Proc IEEE Radio Frequency Integrated Circuits Symp, p.116-119. https://doi.org/10.1109/RFIC.2017.7969031

Wang H, 2015. Radio Channel Measurements and Modeling for Indoor Millimeter-Wave Communications at 45 GHz. PhD Thesis, The Chinese University of Hong Kong, Hong Kong, China.

Wang H, Wang F, Li TW, 2019. Broadband, linear, and high-efficiency mm-Wave PAs in silicon—overcoming device limitations by architecture/circuit innovations. Proc IEEE MTT-S Int Microwave Symp, p.1122-1125. https://doi.org/10.1109/MWSYM.2019.8701025

Wang H, Wang F, Li S, et al., 2020. Power Amplifiers Performance Survey 2000-Present. https://gems.ece.gatech.edu/PA_survey.html

Wang JY, Lan Z, Pyo CW, et al., 2009. Beam codebook based beamforming protocol for multi-Gbps millimeter-wave WPAN systems. *IEEE J Sel Areas Commun*, 27(8):1390-1399. https://doi.org/10.1109/JSAC.2009.091009

Weiß M, Huchard M, Stohr A, et al., 2008. 60-GHz photonic millimeter-wave link for short- to medium-range wireless transmission up to 12.5 Gb/s. *J Lightw Technol*, 26(15): 2424-2429. https://doi.org/10.1109/JLT.2008.927604

Wu XY, Wang CX, Sun J, et al., 2017. 60-GHz millimeter-wave channel measurements and modeling for indoor office environments. *IEEE Trans Antenn Propag*, 65(4): 1912-1924. https://doi.org/10.1109/TAP.2017.2669721

Xu J, Hong W, Jiang ZH, et al., 2017. A Q-band low-profile dual circularly polarized array antenna incorporating linearly polarized substrate integrated waveguide-fed patch subarrays. *IEEE Trans Antenn Propag*, 65(10):5200-5210. https://doi.org/10.1109/TAP.2017.2741065

Yu C, Lu QY, Yin H, et al., 2020. Linear-decomposition digital predistortion of power amplifiers for 5G ultrabroadband applications. *IEEE Trans Microw Theory Techn*, 68(7):2833-2844. https://doi.org/10.1109/TMTT.2020.2975637

Yu SH, Hong W, Zhang Y, 2016. Packaged ultrabroadband terminal antenna for 45 GHz band IEEE 802.11aj applications. *IEEE Trans Antenn Propag*, 64(12):5153-5162. https://doi.org/10.1109/TAP.2016.2608385

Yu XH, Shen JC, Zhang J, et al., 2016. Alternating minimization algorithms for hybrid precoding in millimeter wave MIMO systems. *IEEE J Sel Top Signal Process*, 10(3): 485-500. https://doi.org/10.1109/JSTSP.2016.2523903

Yu YK, Baltus PGM, van Roermund AHM, 2011. Integrated 60GHz RF Beamforming in CMOS. Springer, Dordrecht, USA.

Zhang T, Zhang Y, Cao LN, et al., 2015. Single-layer wideband circularly polarized patch antennas for Q-band applications. *IEEE Trans Antenn Propag*, 63(1):409-414. https://doi.org/10.1109/TAP.2014.2365036

Zhang XZ, Li F, Yang HL, et al., 2019. Cloud VR Solution Sales White Paper. Huawei Technologies Co., Ltd., issue 1.0.

Zhang Y, Xue ZL, Hong W, et al., 2017. Planar substrate-integrated endfire antenna with wide beamwidth for Q-band applications. *IEEE Antenn Wirel Propag Lett*, 16: 1990-1993. https://doi.org/10.1109/LAWP.2017.2692250

Zhang Y, Hong W, Mittra R, 2019. 45 GHz wideband circularly polarized planar antenna array using inclined slots in modified short-circuited SIW. *IEEE Trans Antenn Propag*, 67(3):1669-1680. https://doi.org/10.1109/TAP.2018.2888984

Zhang YP, Mao JF, 2019. An overview of the development of antenna-in-package technology for highly integrated wireless devices. *Proc IEEE*, 107(11):2265-2280. https://doi.org/10.1109/JPROC.2019.2933267

Zhou P, Cheng KJ, Han X, et al., 2018. IEEE 802.11ay-based mmWave WLANs: design challenges and solutions. *IEEE Commun Surv Tutor*, 20(3):1654-1681. https://doi.org/10.1109/COMST.2018.2816920

Zhu DK, Li BY, Liang P, 2017. A novel hybrid beamforming algorithm with unified analog beamforming by subspace construction based on partial CSI for massive MIMO-OFDM systems. *IEEE Trans Commun*, 65(2):594-607. https://doi.org/10.1109/TCOMM.2016.2625794